Science of the Total Environment 619–620 (2018) 1648–1659

Contents lists available at ScienceDirect

Science of the Total Environment

journal homepage: www.elsevier.com/locate/scitotenv

Monitoring of aeolian desertification on the Qinghai-Tibet Plateau from the 1970s to 2015 using Landsat images

Chun-Lai Zhang [a], Qing Li [b,*], Ya-Ping Shen [a], Na Zhou [a], Xue-Song Wang [a], Jiao Li [a], Wen-Ru Jia [a]

[a] State Key Laboratory of Earth Surface Processes and Resource Ecology, MOE Engineering Research Center of Desertification and Blown-sand Control, Faculty of Geographical Science, Beijing Normal University, Xinjiekouwai Street 19, Beijing 100875, China
[b] Hebei Engineering Research Center of Geographic Information Application, Institute of Geographical Sciences, Hebei Academy of Sciences, Xi Street 94, Shijiazhuang, Hebei Province 050011, China

HIGHLIGHTS

- Desertification from 1977 to 2015 in QTP was monitored using Landsat images.
- The spatial-temporal distribution of ADL in different stages was identified.
- The spatial distribution of ADL was controlled by natural and human factors.
- Human activities were responsible for the expansion of ADL before 2000.
- Ecological protection projects and climate change contributed to the reversal of ADL.

GRAPHICAL ABSTRACT

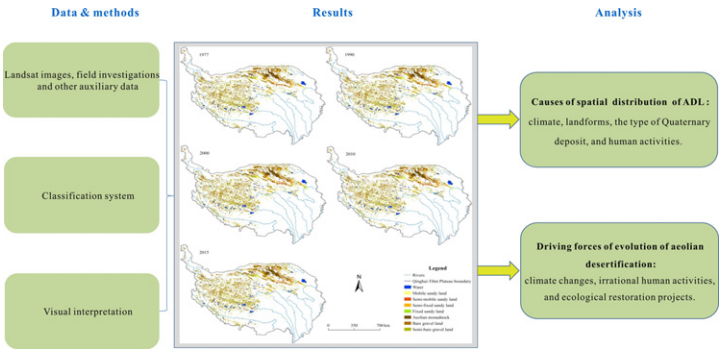

ARTICLE INFO

Article history:
Received 1 July 2017
Received in revised form 23 September 2017
Accepted 14 October 2017
Available online 21 October 2017

Editor: D. Barcelo

Keywords:
Aeolian desertification
Qinghai-Tibet Plateau
Spatial-temporal distribution
Driving force
Landsat images

ABSTRACT

Aeolian desertification, one of the most serious environmental issues, has hampered socioeconomic development on the Qinghai-Tibet Plateau (QTP). However, research on aeolian desertification in this region has been limited. To develop a set of science-based preventive measures to mitigate desertification in this region, it is first necessary to clarify the status, evolution, and driving factors of aeolian desertification. In this study, based on extensive field investigations and a current classification system for aeolian desertification, we established a new system for interpreting aeolian desertified land (ADL) on the plateau using Landsat images from 1977, 1990, 2000, 2010, and 2015 and obtained the distribution of ADL through visual interpretation of the images. The results showed that ADL covered 392,914 km^2 (15.1% of the study area) in 2015, including gravel ADL, sandy ADL, and aeolian monadnocks. Controlled by climate, landforms, the type of Quaternary deposit, and human activities, ADL is scattered throughout the plateau but is concentrated mostly in the western and northern parts. Aeolian desertification on the plateau expanded from 1977 to 2000 and then began to reverse. The evolution during the study period is the result of the combined effects of natural and human factors. Irrational human activities were the dominant factor responsible for the expansion of ADL prior to 2000, whereas the subsequent reversal was mainly caused by climate change combined with large ecological restoration projects.

* Corresponding author at: Hebei Engineering Research Center of Geographic Information Application, Institute of Geographical Sciences, Hebei Academy of Sciences, Xi Street 94, Shijiazhuang, Hebei Province, China.
E-mail address: qingli@mail.bnu.edu.cn (Q. Li).

https://doi.org/10.1016/j.scitotenv.2017.10.137
0048-9697/

1. Introduction

Desertification, a major type of land degradation occurring around the world, has become one of the world's most serious environmental issues (Dregne et al., 1991; UNCED, 1992; Adger et al., 2001; Reynolds et al., 2007). China's QTP is one of the world's most sensitive environments and is experiencing extensive aeolian desertification (Qiu, 2008; Yao et al., 2012). This region is strongly affected by regional atmospheric circulation patterns and the harsh climate created by its high elevation. Most areas of the plateau suffer from a cold and dry climate, resulting in a fragile ecology that creates favorable conditions for aeolian desertification (Li et al., 2001). Under the influence of climate change and human activities, it has become an important area of ADL in China (Li et al., 2010), and desertification has become a serious problem that is hampering socioeconomic development on the plateau (Zhang et al., 2009) and threatening its ecological environment. These changes may even be affecting eastern Asia and the global environment because of its effects on regional air circulation patterns and its role as a water source for most of Asia (Sun et al., 2004; Wang et al., 2004b; Xue et al., 2009).

Monitoring is a prerequisite to understand the distribution, causes, and influence of desertification. There have been a few studies concerning the aeolian desertification in this region. By summarizing the survey results of ADL from former studies (Duan and Shi, 1988; Li et al., 1990), Zhang et al. (2009) found that aeolian desertification on the Qinghai Province was expanding during the period from 1959 to 2004. Li et al. (2010) monitored the aeolian desertification on the Tibet Autonomous Region by interpreting a series of Landsat images, he concluded that the aeolian desertification was in expansion from 1992 to 2004 and was mainly influenced by climate changes and human activities. Using a similar method, Li et al. (2016a, 2016b) found an expansion of aeolian desertification on the Tibet Plateau first and then a reverse during the period of 1977 to 2010. Other documents have been mainly focused on a few hotspots, such as the Yarlung Zangbo River Basin (Dong et al., 1991; Shen and Yang, 1999; Shen et al., 2012), source areas of the Yangtze and Yellow Rivers (Yan et al., 2009; Dong et al., 2009; Hu et al., 2010, 2012, 2015), the Qinghai Lake Basin (Wang et al., 2015) and so forth. However, most of the above investigations are fragmentary their data cannot be integrated to comprehensively reflect the desertification situation for the entire plateau due to between-study inconsistences in the desertification classification system and study period. Furthermore, as most of the studies are based on RS imagery prior to 2010, the latest monitoring results was absent. To comprehensively understand the distribution, causes, and development trend of desertification, it is crucial to obtain the integrated information of spatial distribution and evolution of ADL on the whole plateau.

In this study, we developed a desertification attribute set and established an interpretation index system for use in interpreting Landsat images based on field investigations and the fruits of previous research to identify the distribution and severity of ADL on the plateau from 1977 to 2015. We monitored aeolian desertification to obtain changes in the area and spatial distribution of ADL among five years: 1977, 1990, 2000, 2010, and 2015. Based on the results of this analysis, we discuss changes in the spatial pattern of ADL since 1977 and their underlying causes. Our results will support research on the status, evolution, driving forces, and development trends of aeolian desertification with sequential and integrated data and will therefore contribute to the formulation of appropriate strategies to control desertification on this important plateau.

2. Materials and methods

2.1. Study area and field investigations

The QTP is located in southwestern China (Fig. 1), where it covers an area of 2,603,431 km^2. The elevation is generally greater than 4000 m. Fig. S1 illustrates the topography of the study area. The administrative regions include the Tibet Autonomous Region, Qinghai Province, and parts of the Xinjiang Uygur Autonomous Region and of Gansu, Sichuan, and Yunnan provinces. The plateau is surrounded by high and extensive mountain ranges interlaced with valleys and basins. It is generally warm and wet in the southeast and cold and dry in the northwest. Across the region, the annual average temperature ranges from −5.6 °C to 17.6 °C, and the temperature difference between day and night ranges from 14 °C to 17 °C. The precipitation distribution is uneven. Annual precipitation in the Motuo area, in the southeast, and in the Lenghu area, in the northwest, averages more than 2000 mm and approximately 17.6 mm, respectively. Under the influence of the westerly circulation and the plateau's terrain, annual average wind speed is generally greater than 3.0 m s^{-1} in the northwest, with gales (i.e., a wind speed higher than 17 m s^{-1}) occurring on more than 50 days annually (Li et al., 2001). In the southeast, it decreases to 5 days annually. The mean annual wind velocity, mean annual temperature, and annual precipitation were calculated using meteorological data from the Shiquanhe, Anduo, Geermu, Wudaoliang, and Maduo meteorological stations from 1975 to 2015.

The Plateau's population density is low and is mainly concentrated in cities, towns, and river valleys with good natural conditions for farming. The average regional population density is 5.0 persons per km^2, but in many areas is less than 1.0 person per km^2. Because of the low temperatures and the spatial differences in precipitation, only approximately 12,453 km^2 (0.5% of the total area) are suitable for farming, mostly in the valleys of the Yarlung Zangbo River, Lancang River, Nujiang River, and Yangtze River in the southeastern plateau and the Huanghe River and Huangshui River in the northeast. Animal husbandry is the only agricultural activity in 57 of the plateau's 188 counties, and the area of grazing land totals 1,421,473 km^2 (Lv and Yu, 2011; Zhang et al., 2012), accounting for 54.6% of the total area. Excessive animal grazing is the major human activity that has exacerbated desertification in this region of the plateau (Zhang et al., 2012).

Field investigations were conducted to record the locations of different types of ADL and their distribution, vegetation status, land use type, and surface soil characteristics in 2013, 2014, 2015, and 2016. We carried out field investigation based on four field routes: the route of river valleys in southern Tibet, the route of plateau surfaces in northern Tibet, the route of southern Qaidam Basin-Gonghe Basin, and the route in Zoige Basin. During each survey, we selected 4 to 40 sites for each of the ADL categories along the investigation routes. There are 347 sites in total (Fig. 1). The sites selection should follow several principles. First, the site is typical ADL types (based on the classification of ADL system from Li et al., 2010), and the site area should be larger than 500 m × 500 m. Second, the soil-type and the vegetation-type of each site are homogeneous, and the terrain is relatively flat. Third, these sites are mainly distributed 500 meters away from the road in order to avoid traffic impact. At each site, we recorded the type, severity, spatial distribution, and cause of desertification within an area of 100 m × 100 m. Soil samples were collected to a depth of 5 cm to measure the surface particle size distribution. All records were combined with georeferenced remote sensing images to establish an attribute set, including the color and texture of the images, to guide our subsequent interpretation of ADL from the remote sensing images.

2.2. Data acquisition and pre-processing

We used Landsat images as the main data source for monitoring desertification on the plateau in each part of the study period. June to September is the vegetation-growing season on the plateau, so this stage is ideal to monitor the status of desertification based on the degree of vegetation cover. However, this period is also the rainy season and is frequently cloudy, so it is difficult to obtain images that cover the entire study area with no clouds or few clouds in the same year. To resolve this problem, we selected images from the previous or subsequent

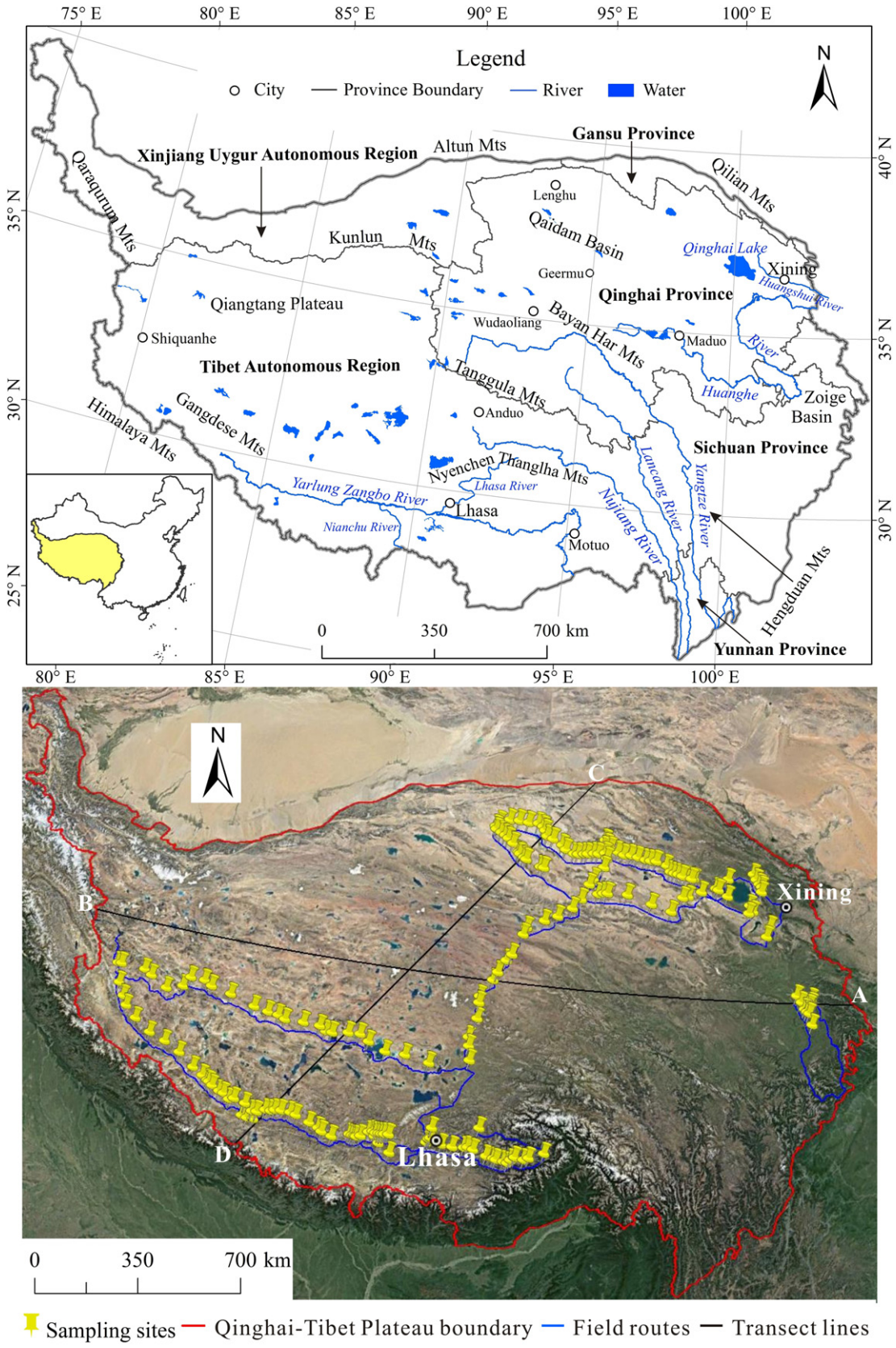

Fig. 1. Location of the QTP and of the field sampling sites from 2013 to 2016. The lines from A to B and from C to D represent the transect lines shown in Figs. 5 and 6, respectively.

year when it was necessary to replace poor-quality images in a given year. Landsat images were limited both in quantity and quality from 1972 to 1985, so high-quality images covered only part of the plateau. During this period, summer Landsat images acquired in 1977 were most abundant and had the highest quality. Thus, we selected 1977 to represent the beginning of our efforts to monitor aeolian desertification.

In total, we obtained 793 Landsat images in 1977 (169), 1990 (156), 2000 (156), 2010 (156), and 2015 (156) suitable for use in monitoring aeolian desertification in the study area. All images were downloaded from the website of the United States Geological Survey (Table 1). To compare Landsat images acquired in various different years, all images were resampled with a 78 m spatial resolution using the nearest neighbor method.

Terrain data utilized in this study was the SRTM digital elevation model (DEM) with a 90 m spatial resolution, which was downloaded from China's Geospatial Data Cloud. Land-use data was obtained from a 1:100,000 land-use database, which included land-use products from 1985, 1995, and 2000; Quaternary sediments data was obtained from a 1:2,500,000 Quaternary Geology database; vegetation-type data was obtained from a 1:1,000,000 vegetation database from 2001 and soil-type data was based on a 1:1,000,000 soil database from 1995. All of the land-use, Quaternary sediments, vegetation-type, and soil-type data were downloaded from the Cold and Arid Regions Science Data Center of China (Table 1). Meteorological data was downloaded from the China Meteorological Data Service Center. After all the data had been collected, we processed the data (clipping, format conversion, and projection coordinate conversion) based on the boundary of the study area. All spatial data were converted into raster data with a 78 m spatial resolution using the Albers equal-area conical projection and WGS-84 datum.

We used an image-matching method based on image features to geometric correct the Landsat images. First, the 2010 images were corrected geometrically using the 1:100,000 topographical map as the reference. We then corrected the Landsat images from 1977, 1990, 2000, and 2015 using the calibrated images from 2010. Specifically, we selected 20 to 50 control points in each image to complete the geometric correction by means of a triangulated irregular network model, and resampled the pixels using bilinear interpolation. Radiometric calibration of the Landsat images was conducted using version 4.7 of ENVI software.

2.3. Classification and grading system for desertification, and interpretation signs

In recent years, many classification index systems have been established to monitor and assess aeolian desertification in China (Wang et al., 2004a; Zeng and Feng, 2005). Among these indicator systems, the system developed by Li et al. (2010) is considered to be suitable for monitoring and assessing the desertification on the QTP (Hu et al., 2015). This system divides aeolian desertification into 10 categories based on a combination of properties, such as surface sediment composition, coverage by shifting sand, vegetation cover, dune morphology, dune waviness, and other factors.

However, the system has two main insufficiencies when using remote sensing data for monitoring desertification. First, because it is possible for sandy grassland to become desertified land when the temperature increases, leading to permafrost degradation, the system fails to account for an important type of land on the plateau that has a high potential for desertification. Second, it is difficult to distinguish monadnock areas from badlands and semi-mobile sandy land from semi-fixed sandy land created by wind erosion in remote sensing images. Consequently, we developed an index system that was more appropriate for interpretation of aeolian desertification in remote sensing images but that was based on Li et al.'s (2010) indicator system. The revised system comprehensively considered surface material composition, vegetation cover, mobile sand area, aeolian landforms, and other landscape features. This indicator system classified aeolian desertified land into the six categories described in Table 2: mobile sandy land, semi-fixed sandy land, fixed sandy land, aeolian monadnocks, bare gravel land, and semi-bare gravel land. In addition, we categorized ADL (except for aeolian monadnocks) into sandy and gravel types according to the characteristics of the surface material: sandy ADL included mobile sandy land, semi-fixed sandy land, and fixed sandy land, whereas gravel ADL included bare gravel land and semi-bare gravel land. The surface sediments of sandy ADL are mainly composed of very fine sand, fine sand, and medium sand, with gravel accounting for less than 10% of the total; in contrast, surface sediments of the gravel ADL contained much more gravel (>10%) and generally a higher content of silts and clays (>17%) (Table S1). Aeolian monadnock is a severe wind-erosion land dominated by extensive wind-eroded hillocks, mounds, unaka, and depressions. The fragmentation degree is above 30%, with little or no vegetation. Table 2 also shows the correspondence between landscape images and remote sensing images obtained from field surveys and the corresponding features of Landsat OLI images (false-color composites) obtained over 4 years (2013–2016), which represent the main interpretation signs for different categories of ADL.

2.4. Method of extracting desertification information and validation

Currently, visual interpretation and automatic classification are the two main methods of monitoring desertification using remote sensing data (Xu, 2009). The visual interpretation method is simple and has good flexibility, high precision and so on; thus it is the most commonly used method (Zeng and Feng, 2005; Kang and Liu, 2014). However, it requires a great deal of manpower and material, and the financial costs are high. The automatic classification method of monitoring desertification includes supervised/unsupervised classification (Li et al., 2010), desertification thematic index (Tucker et al., 1991; Milich and Weiss, 2000; Feng et al., 2016), spectral mixture analysis (Li et al., 2013) and so on. It saves time and labor but is less accurate because a given object may have different spectral characteristics, and different objects can have the same spectral characteristics, especially at larger scales. In this study, we used visual interpretation to monitor aeolian desertification on the QTP.

Table 1
Data sources for the aeolian desertification monitoring and analysis.

	Data category	Spatial resolution or scale	Time	Image quantity	Download site
Remote sensing data	Landsat MSS	78 m	1976–1978	169	http://landsatlook.usgs.gov/
	Landsat TM	30 m	1989–1991	156	http://landsatlook.usgs.gov/
	Landsat ETM +	30 m	1999–2001	156	http://landsatlook.usgs.gov/
	Landsat TM	30 m	2009–2011	156	http://landsatlook.usgs.gov/
	Landsat OLI	30 m	2015	156	http://landsatlook.usgs.gov/
Auxiliary data	SRTM DEM	90 m	2000	18	http://www.gscloud.cn/
	Land-use map	1:100,000	1985		http://westdc.westgis.ac.cn/
	Land-use map	1:100,000	1995		http://westdc.westgis.ac.cn/
	Land-use map	1:100,000	2000		http://westdc.westgis.ac.cn/
	Vegetation-type map	1:1,000,000	2001		http://westdc.westgis.ac.cn/
	Soil-type map	1:1,000,000	1995		http://westdc.westgis.ac.cn/
	Quaternary sediments map	1:2,500,000			http://westdc.westgis.ac.cn/
	Meteorological data		1975–2015		http://data.cma.cn/

Table 2
Classification of ADL, based on a modification of the system of Li et al. (2010), supported by an interpretation index system, and the resulting attribute set for interpreting Landsat images of the QTP.

Category	Proportion of the area covered by gravel (%)	Vegetation cover (%)	Landscape	Tone and texture of Landsat images	Picture of typical landscape	Typical Landsat image (combination of bands near-infrared, red, and green)
Mobile sandy land	<10	<10	Extensive and very intense aeolian activity and widespread sand dunes, including areas with flat sands, dense barchans, dune chains, mobile star dunes, longitudinal dunes, compound dunes, and climbing dunes, mainly in super-xerophytes and strong xerophytes, with sparse desert vegetation, surface material is mainly composed by sands, the soil type is aeolian sandy soil, and the mobile sand area >30%.	Tone is bright white, with clear shapes of shifting sand dunes. There is a wavy texture.		
Semi-fixed sandy land	<10	10–30	Extensive surface wind–sand flow activity, with scattered sand dune distribution, a few patches of mobile sand sheets, mainly in xerophytes and strong xerophytes, a desert or desert grassland landscape, the soil type is aeolian sandy soil, and the mobile sand area ranged from 10 to 30%.	Tone is light pink, with a rough surface texture, and the shapes of sand dunes can be identified.	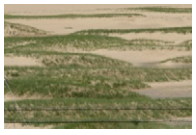	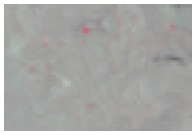
Fixed sandy land	<10	30–50	Obvious traces of wind erosion, with surface wind–sand flow, scattered or sparse sand dunes, fixed flat sands and dunes, and blowout and deposited sand, mainly in xerophytes and intermediate mesophytes, a grassland or desertified grassland landscape, and the mobile sand area ranged from 5 to 10%.	Tone is light red, dotted with darker red spots, and the surface texture is coarse and partially bare.	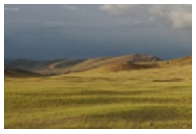	
Aeolian monadnocks		<5	Severe wind erosion, fragmentation degree above 30%, land surface dominated by extensive wind-eroded hillocks, mounds, unaka, depressions induced by wind erosion so that the terrain is fragmentary badland, with few or no vegetation.	Tone is grey-white, with a rough surface texture; monadnocks can be identified clearly.		
Bare gravel land	>10	<10	Erosion has exposed a surface dominated by coarse sand and gravel, with sparse dunes, sheets of gravel and sand, coppice dunes, or locally deposited sand, exposing a Gobi-type landscape.	Tone is off-white, with a smooth surface texture.	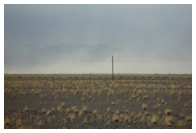	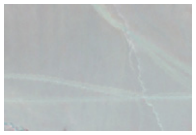
Semi-bare gravel land	>10	10–30	Wind erosion has exposed coarse sands and gravel, with sparse coppice-type dunes or gravel and sand sheets, exposing a desertified grassland landscape and the landscapes have seasonal variation.	Tone is similar to that of fixed sands, but darker due to the higher gravel content, and images have a rough surface texture.		

We interpreted the remote sensing data using ArcGIS 10.0. To achieve the required mapping accuracy, we formulated several guiding principles. First, the minimum mapping unit size was 6 × 6 pixels, and the accuracy of the boundary between patches was limited to 2 pixels to keep the interpretation error rate below 5%. Second, the Landsat images were the key data for monitoring desertification, and the terrain, soil-type, vegetation-type, land-use, and Google Earth data were auxiliary data. That is, we used the established interpretation signs and classification index system to account for the Landsat images, as well as the terrain, soil-type, vegetation-type, land-use, and Google Earth data to classify ADL and locate its boundaries by comparing these multiple information categories to provide an integrated analysis of all useful data. Third, the personnel who perform the classification should validate their colleagues' interpreted results to detect and correct errors; thus, quality control and correction of erroneous results were carried out through peer review.

The accuracy of the interpreted results was tested by means of a combination of field and indoor validation. Field validation was conducted by overlaying the field survey results and the interpreted results, combined with environmental information and landscape photos, to evaluate result accuracy. Afterwards, the properties of each validation point were used to modify incorrectly classified map patches. These validation points included all types of ADL and were evenly spatially distributed. The indoor validation involved the random selection of 10% of the map patches as assessment samples, followed by an assessment of whether their properties and boundary positions were reasonable, based on the field investigation data and high-definition Google Earth images. The interpretation accuracy was the ratio of the number of correctly classified samples to the total number of assessment samples. The interpretation error rate was then equal to 100% minus the interpretation accuracy. If the interpretation error rate was above 5%, we optimized the ADL database to ensure a classification accuracy of better than 95%.

3. Results and analysis

3.1. Spatial distribution of ADL and the controlling factors

3.1.1. Spatial distribution

The results showed that aeolian desertification was widespread on the QTP, but especially in the northern and western parts of the plateau (Fig. 2). In 2015, the area of ADL totaled 392,914 km^2 (Table 3), which amounted to 15.1% of the study area; of this total, 79.1% was primarily bare gravel land (207,431 km^2) and semi-bare gravel land

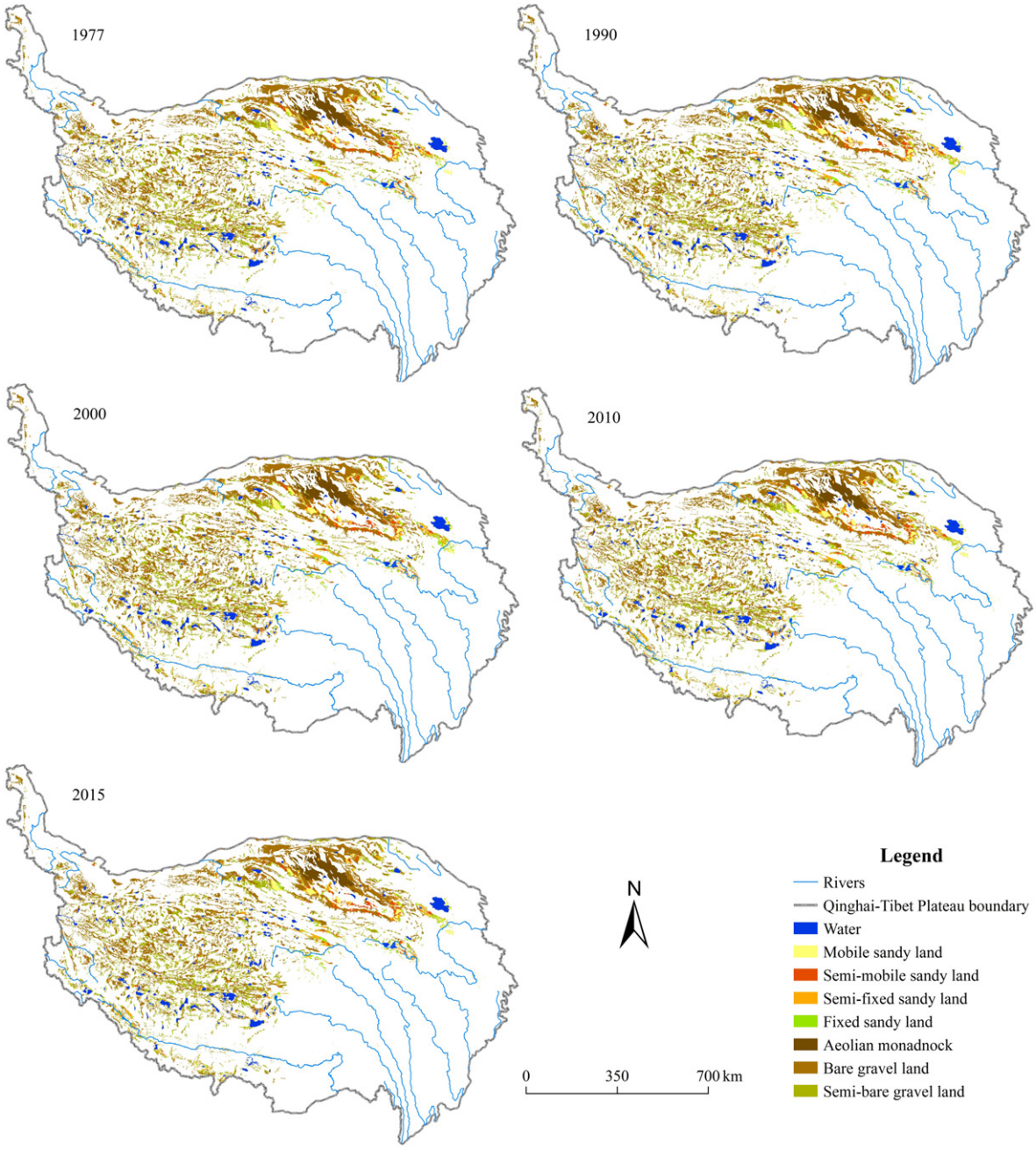

Fig. 2. Distribution of ADL on the QTP from 1977 to 2015. The blank areas on the QTP represent land that is free of ADL.

(103,196 km^2). In the sandy ADL, mobile sandy land occupied the largest area (28,235 km^2), followed by semi-fixed sandy land (21,572 km^2) and fixed sandy land (12,768 km^2). The aeolian monadnocks covered only 5.0% of the total ADL area.

Table 3
Categories and area of ADL on the QTP.

ADL category	Area (km^2)				
	1977	1990	2000	2010	2015
Mobile sandy land	27,096	28,035	29,035	28,534	28,235
Semi-fixed sandy land	21,037	22,113	22,889	21,948	21,572
Fixed sandy land	11,058	12,257	13,421	12,866	12,768
Aeolian monadnocks	19,766	19,853	19,810	19,738	19,712
Bare gravel land	204,327	209,447	212,180	208,328	207,431
Semi-bare gravel land	103,375	105,035	104,272	103,371	103,196
Total	386,659	396,740	401,607	394,785	392,914

In addition to the large and concentrated distribution of ADL in the northern plateau, much of the ADL was scattered throughout the western plateau (Fig. 2). From southeast to northwest, the distribution of ADL changes gradually from sporadic, with small areas, to increasingly frequent patches with larger areas. There is little ADL in the southeastern plateau, where precipitation is high and deeply incised valleys are widespread. ADL was sporadic and was mainly composed of sandy ADL in this area. In the valleys and lake basins of the southern plateau (Fig. 3A) and northeastern plateau (Fig. 3B), sandy ADL was the main category, but the ADL was distributed in patches or discontinuous strips. In the plateau areas of northern Tibet and southern Qinghai, bare and semi-bare gravel land were the dominant categories in large patches (Fig. 3C). In the Qaidam Basin of the northern plateau, large contiguous areas in different categories of ADL were found, including large areas of aeolian monadnocks (Fig. 3D). This area was also the most severely desertified region.

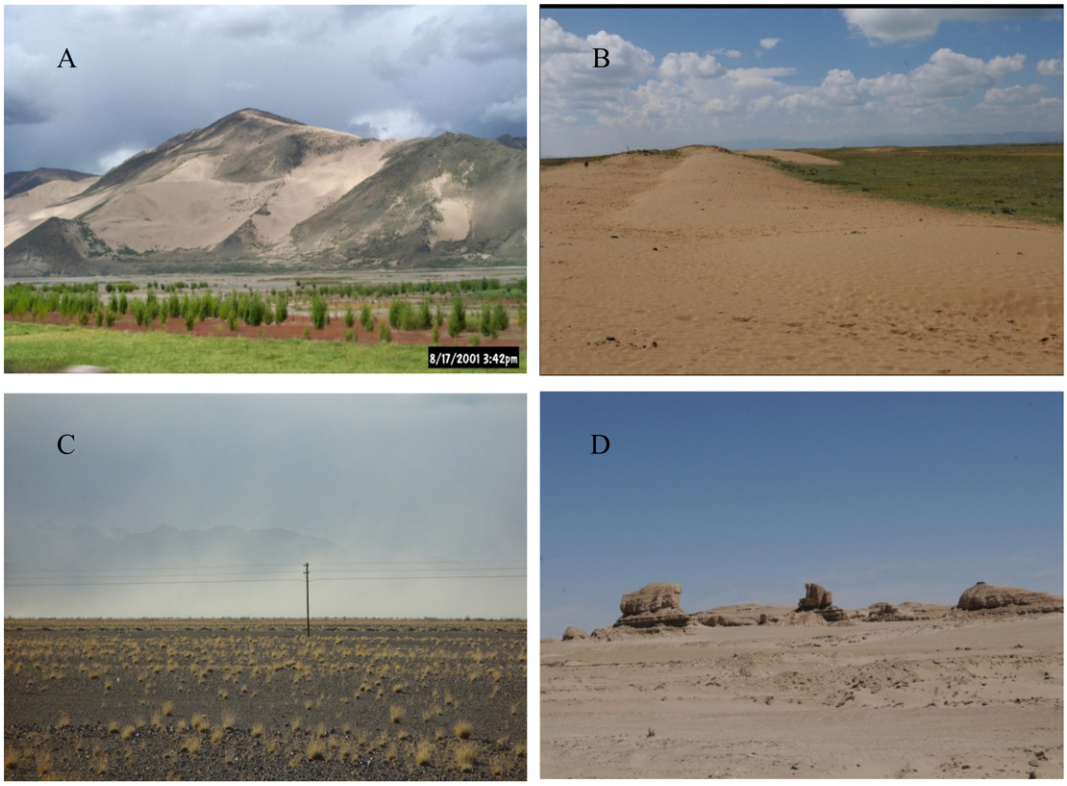

Fig. 3. Typical landscapes of ADL on the QTP: (A) Patches of climbing dunes on hillslopes in the wide valleys of the Yarlung Zangbo River. (B) Sandy ADL in the Zoige Basin in the upper reaches of the Huanghe River, in the northeastern plateau. (C) Gravel ADL on the plateau surface of northern Tibet and southern Qinghai. (D) Aeolian monadnocks in the Qaidam Basin.

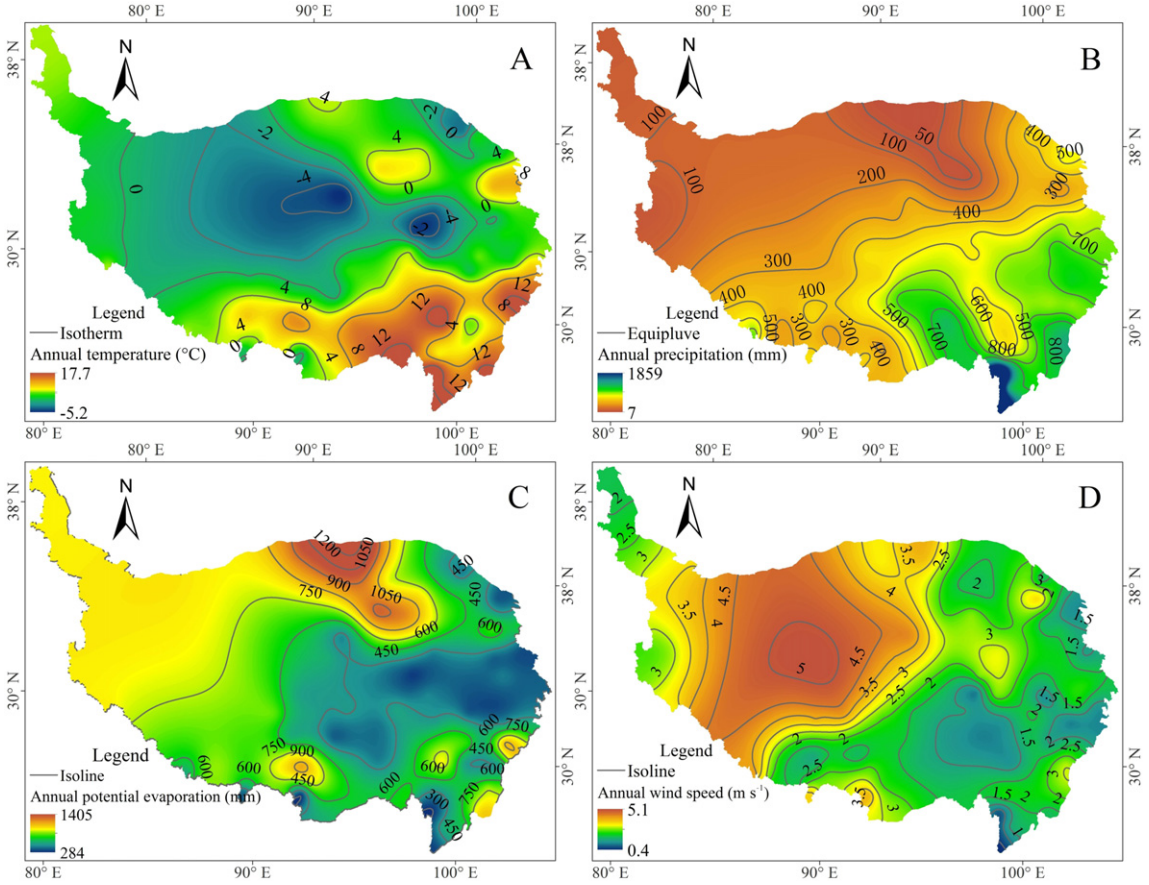

Fig. 4. Spatial distribution of (A) mean annual temperature, (B) total annual precipitation, (C) annual potential evaporation, and (D) mean annual wind speed on the QTP.

3.1.2. Effect of climate on the distribution of ADL

The mean annual temperature decreases from higher than 17 °C in the southeastern regions of the plateau to less than −5 °C in the north-central regions (Fig. 4A). As aeolian desertification occurs mainly in arid, semi-arid, and some semi-humid regions (UNEP, 1994), moisture is a basic factor controlling the spatial range of ADL. With the exception of some moist areas in the southeastern plateau, rainfall on the QTP is generally low, so most of the plateau has a semi-arid to arid climate. Decreasing precipitation (Fig. 4B) and increasing potential evaporation (Fig. 4C) from the southeast to the northwest indicated a progressively drier climate along this direction. Therefore, the climate is relatively warm and wet in the southeast and relatively dry and cold in the northwest. Superimposition of local air circulation patterns on the westerly jet creates a windy environment on the plateau, and gales occur more than 50 days per year in many regions of the plateau (Li et al., 2001). Fig. 4D shows that the strongest winds occur in roughly the same area as the coldest and driest regions.

The combination of drought and a windy climate create favorable conditions for strong erosion on the plateau, with erosivity strengthening from the southeast to the northwest (Dong and Kang, 1994). ADL therefore becomes more and more widespread as it moves in this direction. Table 4 summarizes the area of ADL in each of the main climatic regions. ADL in the plateau's arid regions (with precipitation <200 mm) totaled 252,545 km^2, which amounted to 26.9% of the total arid regions on the plateau. In contrast, ADL in the semi-arid region (with precipitation of 200 to 400 mm), semi-humid region (400 to 800 mm), and humid region (>800 mm) covered 139,250, 1114, and 4 km^2, respectively, which accounted for 14.1, 0.2, and 0.0% of the land areas in each climatic region. These proportions indicate that the arid areas are most susceptible to aeolian desertification, followed by the semi-arid areas. Compared with the semi-arid zone, susceptibility decreases remarkably (by two orders of magnitude) in the semi-humid zone. In the humid zone, aeolian desertification is rare, except for some local and specialized areas such as dry and hot valleys. The consistency of the spatial distribution of ADL with the climate parameters confirms the importance of climate for aeolian desertification on the plateau.

Regionally, under the control of subsidence of airflow on the plateau, the Qaidam Basin has developed a typical extremely arid continental desert climate, with low precipitation, strong evaporation, and strong wind erosion. The basin is covered by desert vegetation and is the most concentrated area of desertification on the QTP. The plateau surface in northern Tibet and southern Qinghai is characterized by a high-elevation and a cold and arid climate, where low and sparse alpine vegetation forms areas of desert grassland and meadow grassland. The fragile ecosystems and strong winds cause this region to have the most widely distributed area of ADL. Most of the southeastern part of the QTP has a semi-arid to semi-humid or even humid climate. As a result, it is covered by forest vegetation systems, and aeolian desertification is only sporadically distributed in local dry and hot valleys. In the Yarlung Zangbo River Basin in the southern plateau and in the upper reaches of the Huanghe River in the northeastern plateau, the climate is generally semi-arid, and alpine meadow grassland vegetation predominates; crop vegetation appears in some river valleys under good water, heat, and soil conditions. Desertification of agricultural land on the plateau is concentrated in these regions, where it has a discontinuous and sporadic distribution along the river valleys (Li et al., 2001).

Table 4
Area of ADL in each climatic region in 2015 and the proportion of the total land area of each region affected by desertification. Precipitation levels: arid, <200 mm; semi-arid, 200 to 400 mm; semi-humid, 400 to 800 mm; humid, >800 mm.

Climate region	Area (km^2)				Proportion of the area accounted for by ADL (%)
	Gravel ADL	Sandy ADL	Aeolian monadnocks	Total	
Arid	203,998	28,835	19,712	252,545	26.9
Semi-arid	106,170	33,080	–	139,250	14.1
Semi-humid	459	655	–	1114	0.2
Humid	–	4	–	4	0.0

3.1.3. Effect of landforms and quaternary sediments on the distribution of ADL

Aeolian desertification on the QTP occurs mainly in the relatively flat Qaidam Basin, on the plateau surface of northern Tibet and southern Qinghai, and in the wide valleys of the large rivers. With a huge area of flat and open terrain, the Qaidam Basin contains abundant deposits of loose Quaternary sediments. The core area of the basin is mainly composed of lacustrine sediments and salinized sediments, but alluvial, diluvial, and aeolian sediments are mainly distributed in the surrounding piedmont alluvial slopes (Fig. S2). Except for the lacustrine and salinized sediments, the other deposits are rich in sandy material, and the resulting loose texture makes them highly susceptible to wind erosion.

The plateau surface in northern Tibet and southern Qinghai is intact because no rivers have created deep river valleys, so these surfaces are dominated by high terrain and mountains alternating with basins and lakes. A large amount of loose Quaternary sediments has been deposited within the lake and mountain basins, including lacustrine sediments, diluvial sediments, and residues produced by freeze–thaw cycles. Controlled by the landform and ground sediments, ADL in this area is widespread and occurs in large patches.

In the Yarlung Zangbo River Basin and the upper reaches of the Huanghe River, the sediment carried by running water during the flood seasons has accumulated in the wide valleys; during the dry season, sands on the floodplains and low terraces are exposed to the wind and become the source material for aeolian activity. Thus, desertification develops in the high terraces or on hillslopes, where blown sands are deposited along the wide valleys in small, discontinuous patches.

These findings suggest that landform is an important factor that controls the spatial distribution of ADL on the Qinghai-Tibetan Plateau. To further analyze the landform characteristics associated with ADL, we selected two cross-sections through the study area that included obvious changes in topography and different types of ADL. The first transect runs along the 34° N latitude line from the western to the eastern edges of the plateau (Fig. 5). The second runs along an azimuth of 238°, from the northeastern edge of the plateau at 95° E to the southwestern edge at 85° E (Fig. 6).

Along the 34° N latitude line, ADL covered 16.4% of the cross-section, with sandy ADL and gravel ADL accounting for 16.4 and 83.6% of the total ADL, respectively. When this information is combined with the 1:4,000,000 Digital Geomorphologic Map of China (http://westdc.westgis.ac.cn), it can be seen that ADL is distributed mainly in the western part of the cross-section, between the Qaraqurum Mountains and the Tanggula Mountains, where the terrain is high (elevations >4500 m asl) and is characterized by alternating mountains and basins. In the eastern part, the amount of ADL decreases greatly, and the remaining ADL is concentrated in the inter-mountain basins and on the terraces of river valleys. Along the cross-section that runs from the plateau's northern edge at 95° E to its southern edge at 85° E, the area of ADL totaled 32.0% of the cross-section; of this total, the aeolian monadnocks, sandy ADL, and gravel ADL accounted for 17.8, 13.4, and 68.8% of the total, respectively. In the northern part of this cross-section, ADL was concentrated in the Qaidam Basin, and accounted for 50% of the total ADL. In the middle and southern parts, most of the ADL was distributed discontinuously in the basins and piedmont plains that lie between the Kunlun Mountains, Tanggula Mountains, and Gangdese Mountains. In the section south of the Gangdese Mountains, ADL is sporadically distributed in the river valleys.

The processes responsible for aeolian desertification differ among the various Quaternary deposits (Li, 2006). Residues from freeze–thaw weathering, diluvial deposits, and alluvial deposits are generally coarse-textured and poorly sorted (Xiang, 2013). Fine particles in

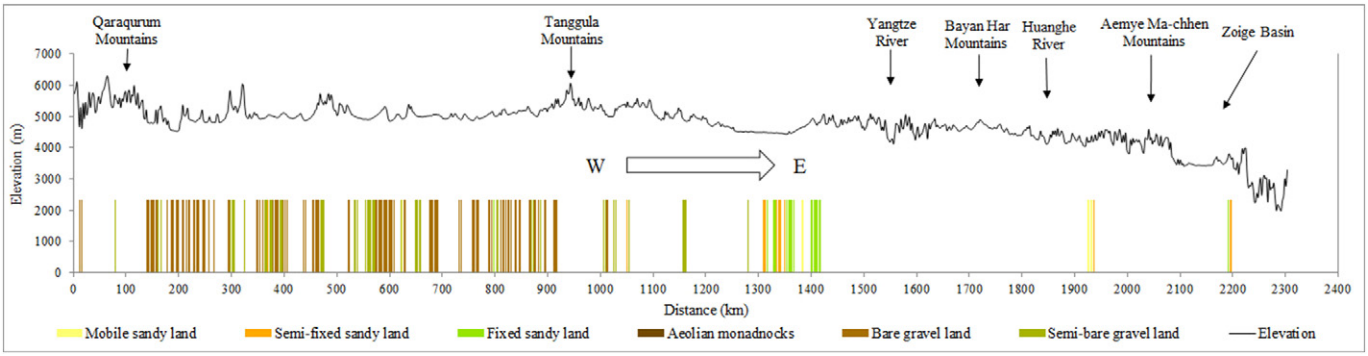

Fig. 5. Distribution of ADL along the 34°N latitude line from west to east on the QTP.

these deposits are prone to be blown away and transported to downwind areas by the region's strong winds. Long-term wind erosion has preserved surface deposits of coarse residues, leading to the development of gravel ADL in the piedmont alluvial-diluvial fans in the Qaidam Basin and in the intermountain basins on the plateau surface of northern Tibet and southern Qinghai. Alluvial, lacustrine, and aeolian sediments are generally fine-grained, well sorted, and loose (Xiang, 2013). Where precipitation and temperatures are low, or where unsustainable human activities occur (e.g., overgrazing), these sediments are vulnerable to wind erosion and aeolian desertification. The extensive distribution of sandy ADL in the alluvial and aeolian areas of the central Qaidam Basin, on lakeside terraces on the plateau surface of northern Tibet and southern Qinghai, and on lakeside terraces and flood plains of wide river valleys in the eastern and southern plateau is obviously controlled by the distribution of the alluvial, lacustrine, and aeolian sediments. Therefore, the genetic types of the Quaternary sediments both restrict the material basis of aeolian desertification and determine the types of desertification.

3.1.4. Effects of human activity on the distribution of ADL

The population density of the QTP is low with 96.3% of the area showing population density less than 20 person km^{-2}, but the regional differences are large (Fig. 7). The population is mainly distributed in the "one river" (Yarlung Zangbo River) and "two reaches" (Lhasa River and Nianchu River) watersheds, in the watershed of the Huanghe River, in the area of the Western Sichuan-Northwestern Yunnan and so on (Fig. 7), where the water and heat conditions are relatively good and can support agriculture and animal husbandry (Zhang et al., 2012). In these areas with intense human activities, the ADL area is 759 km^2, accounting for only 0.2% of the total ADL area, and the ADL mainly distributed in discontinuous strips in the river valley (Fig. 2). These areas mainly have relatively good natural conditions. As a result of unsustainable human activities such as grassland reclamation, overgrazing, and deforestation, the natural vegetation has been destroyed in many areas, leading to the exposure of an increasingly large area of bare soil to the wind, leading to large amounts of wind erosion and aeolian desertification (Zhang et al., 2009; Li et al., 2010). ADL in these areas is thus deeply branded by human activities. In contrast, on the plateau surfaces of northern Tibet and southern Qinghai and in the Qaidam Basin, the population density is low (Fig. 7), and the natural conditions, such as climate, natural vegetation cover, and terrain, are poor. The harsh natural conditions are favorable for aeolian desertification. The ADL area is large, accounting for 99.8% of the total ADL area, and the ADL distributes widely in these areas (Fig. 2). Therefore, the distribution of ADL was mainly determined by natural conditions. The effect of human activities was relatively minor.

3.2. Temporal variation of ADL and its causes

3.2.1. Temporal variation of ADL

From 1977 to 2015, ADL on QTP expanded by 6255 km^2, which is equal to 1.6% of the total ADL in 1977. In other words, the area of desertification on the plateau increased by 165 km^2 annually (Table 5). However, aeolian desertification did not intensify continuously. A transformation occurred between exacerbation of desertification (ADL expansion) and its reversal (ADL contraction), and the rates of expansion or reversal differed during the study period. From 1977 to 1990, ADL expanded rapidly, at 775 km^2 per year. Then, from 1990 to 2000, ADL still increased, but more slowly (at 487 km^2 per year). From 2000 to 2010, ADL began to decrease rapidly, at 682 km^2 per year. The decrease continued from 2010 to 2015, though at the slower rate of 374 km^2 per year. Accordingly, aeolian desertification on QTP expanded from 1977 to 2000, but thereafter it began to decrease.

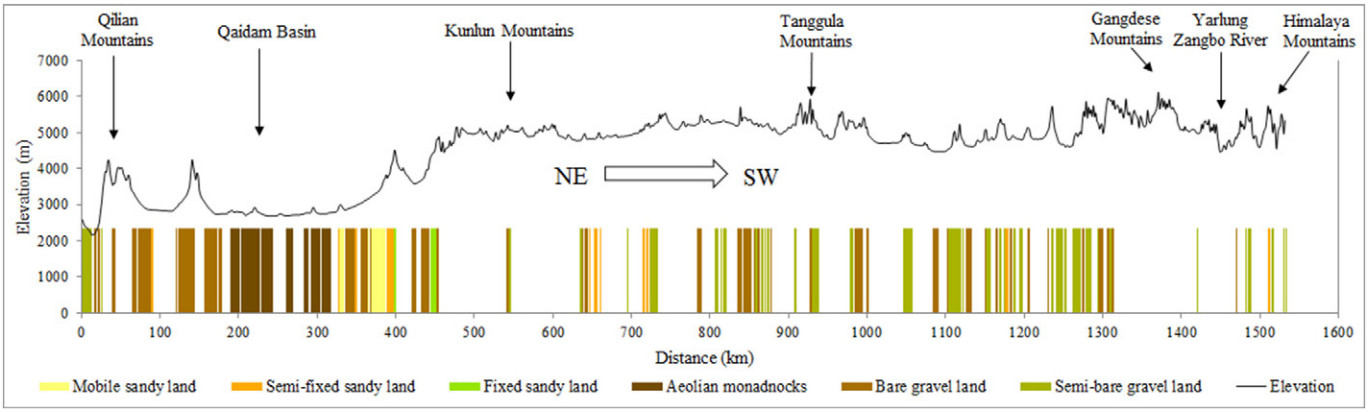

Fig. 6. Distribution of ADL along the transect that runs from the northeastern edge of the plateau at 95°E to the southwestern edge at 85°E.

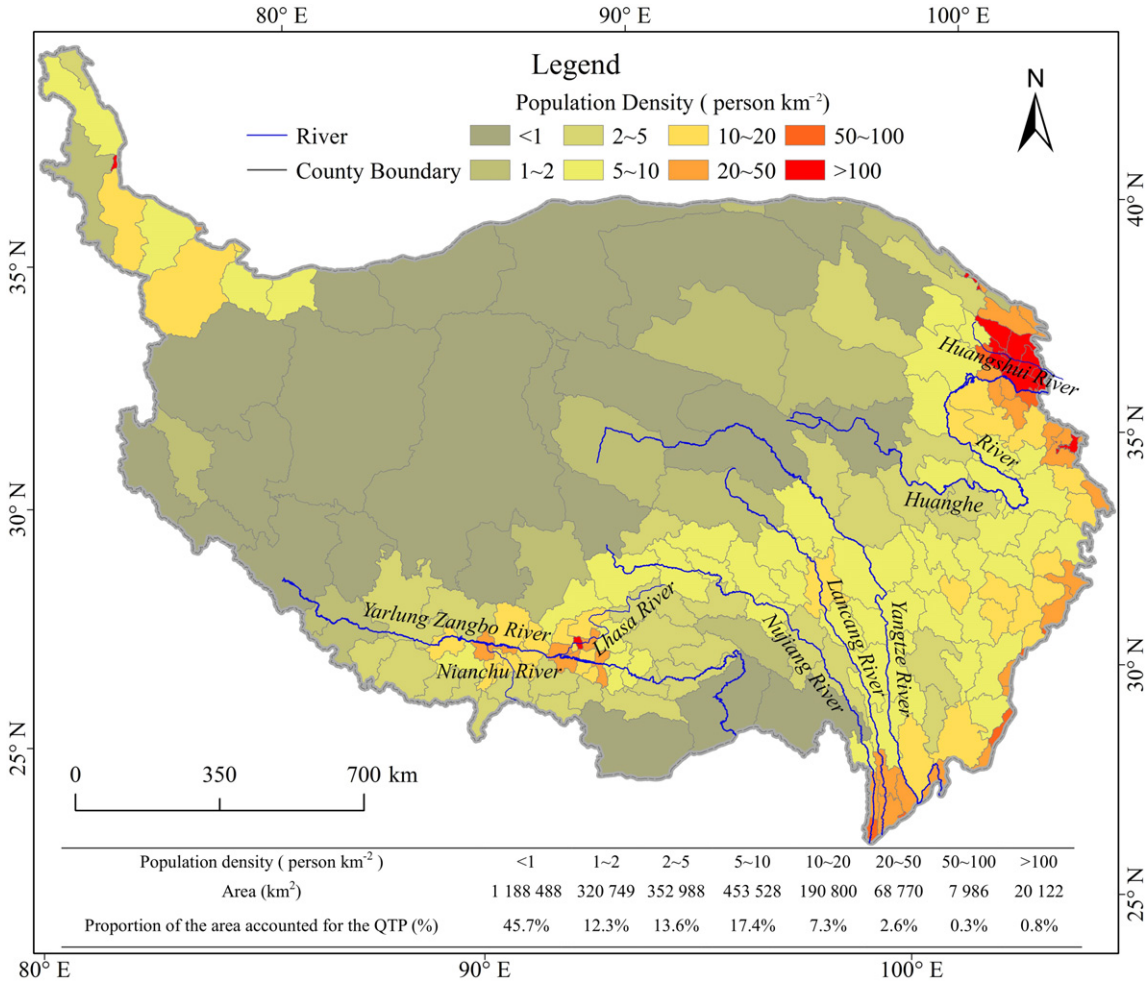

Fig. 7. Spatial distribution of population density on the QTP in 2015. The population density was calculated using county population divided by county area. The county population was obtained from the National Bureau of Statistics of China in 2016.

Graphical superposition of the ADL distribution maps for 2000 and 1977 shows that the expansion of aeolian desertification during this period resulted mainly from the transformation of 7682 km^2 of semi-bare gravel land into bare gravel land, and the transformation of 12,667 km^2 of non-ADL into semi-bare gravel land or fixed sandy land. At the same time, some patches (46 km^2) of sandy ADL converted into other categories and 2441 km^2 of the ADL reversed into non-ADL. Similar graphical superposition shows that although there was a 2172 km^2 expansion of ADL in some areas from 2000 to 2015, 3521 km^2 of bare gravel land and 2644 km^2 of semi-bare gravel land reversed into non-ADL, and 2414 km^2 of bare gravel land changed into semi-bare gravel land, which was the main form of the reversal of aeolian desertification in this period.

3.2.2. Causes of the evolution of aeolian desertification since 1977

Climate change and human activities are the two major driving forces responsible for aeolian desertification (UNEP, 1994; Wessels et al., 2004; Wang et al., 2006, 2012). Among the climate factors, wind, temperature, and rainfall play crucial roles (Lancaster and Helm, 2000; Wang et al., 2005; Yan et al., 2009). In this study, we collected climatic data from five meteorological stations on the QTP during the study period and analyzed the trends in annual mean wind velocity, annual mean temperature, and annual precipitation at these stations using linear regression (Fig. 8).

During the monitoring period, the annual mean temperature and the annual precipitation both increased significantly (Fig. 8); thus, the QTP experienced an overall warming and wetting trend, which correlates with previous research (Liu et al., 2014; Shen et al., 2015; Duan et al.,

Table 5
Changes in the area of ADL on the QTP from 1977 to 2015.

Category	Change in area (km^2)				
	1977–1990	1990–2000	2000–2010	2010–2015	1977–2015
Mobile sandy land	939	1000	−501	−299	1139
Semi-fixed sandy land	1076	776	−941	−376	535
Fixed sandy land	1199	1164	−555	−98	1710
Aeolian monadnocks	87	−43	−72	−26	−54
Bare gravel land	5120	2733	−3852	−897	3104
Semi-bare gravel land	1660	−763	−901	−175	−179
Total	10,081	4867	−6822	−1871	6255

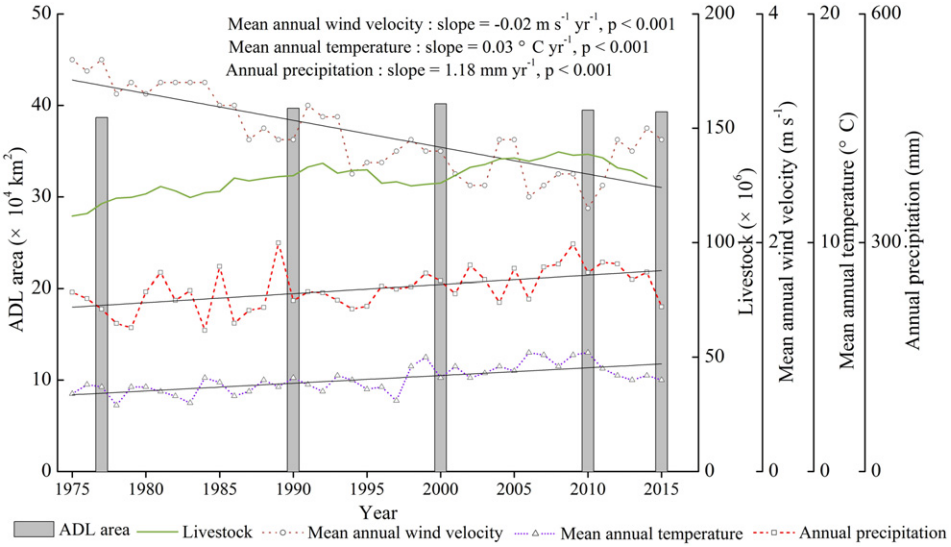

Fig. 8. Changes in the mean annual wind velocity, mean annual temperature, annual precipitation, total number of livestock, and area of ADL on the QTP from 1977 to 2015. The mean annual wind velocity, mean annual temperature, and annual precipitation were calculated using meteorological data from the Shiquanhe, Anduo, Geermu, Wudaoliang, and Maduo meteorological stations from 1975 to 2015. The total number of livestock was obtained from the National Bureau of Statistics of China from 1975 to 2014.

2016). The increasing temperature, along with eased thermal constraints on vegetation growth in QTP, is conducive to vegetation growth (Gao et al., 2013; Yan et al., 2015). Different scholars have reached different conclusions concerning the effect of precipitation on vegetation due to differences in selected meteorological stations and time range (Gao et al., 2013; Sun et al., 2013; Huang et al., 2016). As most of the QTP belong to arid and semi-arid climate and precipitation is a limiting factor for vegetation growth (Sun et al., 2013; Huang et al., 2016), increasing precipitation is conducive to vegetation growth (Li et al., 2016a, 2016b). The annual mean wind velocity decreased significantly (Fig. 8). Since wind erosion is proportional to the third power of wind speed (Wu, 2003), the decreasing wind force should have greatly weakened a key driving force for aeolian desertification. Therefore, taken together, these climate changes were favorable for the mitigation of aeolian desertification. However, the results presented in the previous sections demonstrate that aeolian desertification expanded during most of the early part of the study period, with reversal of desertification mainly occurring since 2000 (Fig. 8). This suggests that human activities were responsible for the increased aeolian desertification, particularly early in the study period.

Grazing is the primary human activity that affects aeolian desertification on the QTP (Chen et al., 2014; Li et al., 2016a, 2016b), and livestock numbers could be used to indicate grazing pressure on grassland. We recorded the total number of livestock and assessed its impact on aeolian desertification (Fig. 8). From 1975 to 1992, the number of livestock increased continuously, reaching levels (52 sheep unit km^{-2}) that greatly exceeded the carrying capacity (45 sheep unit km^{-2}) of the meadows (Ma, 1993). The number of livestock decreased slightly from 1992 to 2000. From 2000 to 2014, the number of livestock initially increased and then decreased (Fig. 8). However, the carrying capacity was still greatly exceeded in many meadows (Shao and Cai, 2008; Shen et al., 2015). Overgrazing damaged the natural vegetation and the soil structure, thereby making the soil more vulnerable to the development of aeolian desertification. Additionally, other irrational human activities, such as grassland reclamation and deforestation, are common on the QTP. These activities also damaged the natural vegetation and the soil, making the soil more vulnerable to the development of aeolian desertification. Therefore, irrational human activities, such as overgrazing, are the main reason for the development of aeolian desertification during those periods.

Since 1999, a series of ecological restoration projects (such as The Grain for Green Project, Grazing Withdrawal Program, Construction of a National Ecological Security Barrier to Protect the Tibetan Plateau, and others) have been implemented throughout the plateau (Li et al., 2016a, 2016b). These projects have applied numerous measures to combat desertification. These measures include fencing of pasture to protect natural vegetation from overgrazing, creating shelter forest systems to protect degraded land from the wind, conversion of some land from cultivation or grazing into forests or artificial grasslands, and providing ecological compensation payments to local residents who were willing to give up animal husbandry or raise their animals in a barn (Li et al., 2010; Chen et al., 2014). These measures proved to be effective in promoting the restoration of vegetation cover and soil fertility, both of which promote the mitigation of aeolian desertification (Zuo et al., 2009; Zhao et al., 2011; Chen et al., 2014). Thus, the aeolian desertification gradually recovered under heavy grazing pressure after 2000, very likely owing to multiple restoration measures. The recovery of desertified land was due to a combination of favorable climate changes (Fig. 8) and ecological restoration projects during this period.

4. Conclusions

ADL on the Qinghai-Tibet Plateau totaled 392,914 km^2 in 2015, accounting for 15.1% of the total land area; of this total, gravel ADL, sandy ADL, and aeolian monadnocks accounted for 79.1, 15.9, and 5.0% of the total area, respectively. The area of bare gravel ADL, aeolian monadnocks, and mobile and semi-fixed sandy ADL totaled 276,950 km^2; thus, aeolian desertification remains a serious problem.

Aeolian desertification on the plateau was controlled by climate, landforms, the type of the Quaternary deposits, and human activity, which have had different relative strengths in different parts of the plateau. ADL is scattered throughout the plateau but is concentrated mostly in the western and northern parts. From the southeast to the northwest, ADL changes gradually from small areas with a sporadic distribution to larger and more continuous areas.

Aeolian desertification on the QTP has changed from expansion to reversal since 1977. From 1977 to 2000, aeolian desertification expanded throughout the plateau, and irrational human activity was the dominant factor responsible for the expansion of ADL. Since 2000, reversal of desertification was the dominant process, and the ADL area decreased gradually. The reversal of aeolian desertification was mainly caused by climate changes that benefited vegetation recovery and decreased wind erosion, as well as by ecological restoration projects.

Despite our promising results, our study has some limitations. The dynamics of desertification, climate change, and human activities vary widely across the QTP. Thus, to control aeolian desertification more effectively, it will be necessary to analyze the dynamics and the dominant factors responsible for desertification more precisely to obtain the details for each area of the QTP.

Acknowledgments

This work was supported by the National Basic Research Program of China (Grant no. 2013CB956001). We appreciate Master's students Peixin Wang and Qin Yang of Heibei Normal University for their help in the visual interpretation work.

Appendix A. Supplementary data

Supplementary data to this article can be found online at https://doi.org/10.1016/j.scitotenv.2017.10.137.

References

Adger, W.N., Benjaminsen, T.A., Brown, K., Svarstad, H., 2001. Advancing a political ecology of global environmental discourses. Dev. Chang. 32, 681–715.
Chen, B.X., Zhang, X.Z., Tao, J., Wu, J., Wang, J.S., Shi, P.L., Wang, J.S., Zhang, Y.J., Yu, C.Q., 2014. The impact of climate change and anthropogenic activities on alpine grassland over the Qinghai-Tibet Plateau. Agric. For. Meteorol. 189, 11–18.
Dong, Y.X., Kang, G.D., 1994. Study on the wind erosion climatic erosivity in arid and semi-arid in China. J. Soil Water Conserv. 3, 1–7 (in Chinese with English abstract).
Dong, Y.X., Jin, Q., Shao, L.Y., 1991. Distribution of the land desertification in Yarlung Zangbo River and its two tributaries in Tibet. J. Desert Res. 11, 59–61 (in Chinese with English abstract).
Dong, Z.B., Hu, G.Y., Yan, C.Z., Wang, W.L., Lu, J.F., 2009. Aeolian desertification and its causes in the Zoige Plateau of China's Qinghai-Tibetan Plateau. Environ. Earth Sci. 59 (8), 1731–1740.
Dregne, H., Kassas, M., Rozanov, B., 1991. A new assessment of the world status of desertification. J. Anim. Sci. 69, 2463–2471.
Duan, G.Q., Shi, M.Y., 1988. General situation of desert and its control in Qinghai province. J. Desert Res. 8 (3), 69–74 (in Chinese).
Duan, A.M., Xiao, Z.X., Wu, G.X., 2016. Characteristics of climate change over the Tibetan Plateau under the global warming during 1979–2014. Clim. Change Res. 12, 374–381 (in Chinese with English abstract).
Feng, L.L., Jia, Z.Q., Li, Q.X., 2016. The dynamic monitoring of aeolian desertification land distribution and its response to climate change in northern China. Sci. Rep. 6, 39563.
Gao, Y.H., Zhou, X., Wang, Q., Wang, C.Z., Zhan, Z.M., Chen, L.F., Yan, J.X., Qu, R., 2013. Vegetation net primary productivity and its response to climate change during 2001–2008 in the Tibetan Plateau. Sci. Total Environ. 444 (1), 356–362.
Hu, G.Y., Dong, Z.B., Lu, J.F., Yan, C.Z., 2010. Aeolian desertification monitoring in the Source Region of Yellow River by remote sensing technology. International Conference on Information Science and Engineering. IEEE, pp. 3506–3509.
Hu, G.Y., Dong, Z.B., Lu, J.F., Yan, C.Z., 2012. Driving forces responsible for aeolian desertification in the source region of the Yangtze River from 1975 to 2005. Environ. Earth Sci. 66 (1), 257–263.
Hu, G.Y., Dong, Z.B., Lu, J.F., Yan, C.Z., 2015. The developmental trend and influencing factors of aeolian desertification in the Zoige Basin, eastern Qinghai–Tibet Plateau. Aeolian Res. 19, 275–281.
Huang, K., Zhang, Y.J., Zhu, J.T., Liu, Y.J., Zu, J.X., Zhang, J., 2016. The influences of climate change and human activities on vegetation dynamics in the Qinghai-Tibet Plateau. Remote Sens. 8 (10), 876.
Kang, W.P., Liu, S.L., 2014. A review of remote sensing monitoring and quantitative assessment of aeolian desertification. J. Desert Res. 34, 1222–1229 (in Chinese with English abstract).
Lancaster, N., Helm, P., 2000. A test of a climatic index of dune mobility using measurements from the southwestern United States. Earth Surf. Process. Landf. 25, 197–207.
Li, P.Z., 2006. Study on Geological Environment of Formation and Development of Desertification in North China. PhD Dissertation. Northwest University, Xi'an, China (in Chinese with English abstract).
Li, C.Z., Shun, B., Lu, J.H., 1990. Investigation on the present status of desert and its developmental tendency Qinghai Province. J. Desert Res. 10 (4), 38–45 (in Chinese with English abstract).
Li, S., Dong, Y.X., Dong, G.R., 2001. Sandy Desertification Problem and Sustainable Development in Qinghai-Tibet Plateau. China Tibetology Publishing House, Beijing (in Chinese).
Li, S., Yang, P., Dong, Y.X., Wei, X.H., Zhang, C.L., 2010. Sandy Desertification and Its Control in Tibet. Science Press, Beijing (in Chinese).
Li, J.Y., Yang, X.C., Jin, Y.X., Yang, Z., Huang, W.G., Zhao, L.N., Gao, T., Yu, H.D., Ma, H.L., Qin, Z.H., Xu, B., 2013. Monitoring and analysis of grassland desertification dynamics using Landsat images in Ningxia, China. Remote Sens. Environ. 138, 19–26.
Li, Q., Zhang, C.L., Shen, Y.P., Jia, W.R., Li, J., 2016a. Developing trend of aeolian desertification in China's Tibet Autonomous Region from 1977 to 2010. Environ. Earth Sci. 75 (10).
Li, Q., Zhang, C.L., Shen, Y.P., Jia, W.R., Li, J., 2016b. Quantitative assessment of the relative roles of climate change and human activities in desertification processes on the Qinghai-Tibet Plateau based on net primary productivity. Catena 147, 789–796.
Liu, S.L., Zhao, H.D., Dong, S.K., An, N.N., Su, X.K., Zhang, X., 2014. Climate changes in the alpine grassland nature reserves on Qinghai-Tibet Plateau in recent 50 years based on SPEI index. Ecol. Environ. Sci. 23, 1883–1888 (in Chinese with English abstract).
Lv, C.H., Yu, B.H., 2011. The Control Technique and Mode of Land Degradation in Qinghai-Tibet Plateau. Science Press, Beijing (in Chinese).
Ma, C.J. (1993). Characteristics and productivity of the grassland in Tibetan Plateau. Inner Mongolia Pratac., Z1, 43–45 (in Chinese).
Milich, L., Weiss, E., 2000. GAC NDVI interannual coefficient of variation (CoV) images: ground truth sampling of the Sahel along north-south transects. Int. J. Remote Sens. 21 (2), 235–260.
Qiu, J., 2008. China: the third pole. Nature 454, 393–396.
Reynolds, J., Smith, D., Lambin, E., Turner, B.N., Mortimore, M., Batterbury, S., Downing, T., Dowlatabadi, H., Fernández, R., Herrick, J., Huber-Sannwald, E., Jiang, H., Leemans, R., Lynam, T., Maestre, F., Ayarza, M., Walker, B., 2007. Global desertification: building a science for dryland development. Science 316, 847–851.
Shao, W., Cai, X.B., 2008. Grassland degradation and its formation causes analysis in Tibetan Plateau. Sci. Soil Water Conserv. 6, 112–116 (in Chinese with English abstract).
Shen, W.S., Yang, P., 1999. Land desertification and its developing trend in Lhasa Area of Tibet. J. Desert Res. 19, 33–37 (in Chinese with English abstract).
Shen, W.S., Li, H.D., Sun, M., Jiang, J., 2012. Dynamics of aeolian sandy land in the Yarlung Zangbo River basin of Tibet, China from 1975 to 2008. Glob. Planet. Chang. 86–87, 37–44.
Shen, W.S., Zhao, W., Wang, X.D., Xu, L.Y. (2015). Ecological Carrying Capacity and Sustainable Development in Tibet. Beijing: China Environmental Press (in Chinese).
Sun, Q.W., Xue, X., Wang, T., 2004. Desertification of northeast Tibetan Plateau grassland and its significance. World Water and Environmental Resources Congress, pp. 1–11.
Sun, J., Cheng, G.W., Li, W.P., Sha, Y.K., Yang, Y.C., 2013. On the variation of NDVI with the principal climatic elements in the Tibetan Plateau. Remote Sens. 5 (4), 1894–1911.
Tucker, C.J., Dregne, H.E., Newcomb, W.W., 1991. Expansion and contraction of the Sahara Desert from 1980 to 1990. Science 253 (5017), 299–300.
UNCED, 1992. Managing Fragile Ecosystems: Combating Desertification and Drought. United Nations Conference on Environment and Development.
UNEP, 1994. Development of guidelines for assessment and mapping of desertification and degradation in Asia/Pacific. United Nations Environment Programme. Proceedings of Draft Report of the Expert Panel Meeting. United Nations Environment Programme, Nairobi, Kenya.
Wang, X.M., Dong, Z.B., Zhang, J.W., Liu, L.C., 2004a. Modern dust storms in China: an overview. J. Arid Environ. 58, 559–574.
Wang, B.F., Liu, X.C., Wang, J.H., Ding, G.D., 2004b. Study on monitoring and assessment indicator systems of sandy desertification in China. J. Arid Land Resour. Environ. 18, 23–28 (in Chinese with English abstract).
Wang, X.M., Dong, Z.B., Yan, P., Zhang, J.W., Qian, G.Q., 2005. Wind energy environments and dunefield activity in the Chinese deserts. Geomorphology 65, 33–48.
Wang, X.M., Chen, F.H., Dong, Z.B., 2006. The relative role of climatic and human factors in desertification in semiarid China. Glob. Environ. Chang. 16, 48–57.
Wang, T., Yan, C.Z., Song, X., Xie, J.L., 2012. Monitoring recent trends in the area of aeolian desertified land using Landsat images in China's Xinjiang Region. ISPRS J. Photogramm. Remote Sens. 68, 184–190.
Wang, H.B., Ma, M.G., Geng, L.Y., 2015. Monitoring the recent trend of aeolian desertification using Landsat TM and Landsat 8 imagery on the north-east Qinghai–Tibet Plateau in the Qinghai Lake basin. Nat. Hazards 79, 1753–1772.
Wessels, K., Prince, S., Frost, P., Van Zyl, D., 2004. Assessing the effects of human-induced land degradation in the former homelands of northern South Africa with a 1 km AVHRR NDVI time-series. Remote Sens. Environ. 91, 47–67.
Wu, Z. (2003). Geomorphology of Wind-Drift Sands and Their Controlled Engineering. Beijing: Science Press(in Chinese).
Xiang, S.Y., 2013. Quaternary Geology and Geomorphological Maps and the Explanation of Qinghai-Tibet Plateau and Its Adjacent Areas. China University of Geosciences Press, Wuhan (in Chinese).
Xu, D.Y., 2009. Quantitative Assessment of the Relative Role of Climate Change and Human Activities in Sandy Desertification—A Case Study in Ordos Plateau, China. PhD Dissertation. Nanjing Agricultural University, Nanjing, China (in Chinese with English abstract).
Xue, X., Guo, J., Han, B.S., Sun, Q.W., Liu, L.C., 2009. The effect of climate warming and permafrost thaw on desertification in the Qinghai-Tibetan Plateau. Geomorphology 165, 182–190.
Yan, C.Z., Song, X., Zhou, Y.M., Duan, H.C., Li, S., 2009. Assessment of aeolian desertification trends from 1975's to 2005's in the watershed of the Longyangxia Reservoir in the upper reaches of China's Yellow River. Geomorphology 112, 205–211.
Yan, L., Zhou, G.S., Wang, Y.H., Hu, T.Y., Sui, X.H., 2015. The spatial and temporal dynamics of carbon budget in the alpine grasslands on the Qinghai-Tibetan Plateau using the Terrestrial Ecosystem Model. J. Clean. Prod. 107 (3), 195–201.
Yao, T.D., Thompson, L.G., Mosbrugger, V., Zhang, F., Ma, Y.M., Luo, T.X., Xu, B.Q., Yang, X.X., Joswiak, D.R., Wang, W.C., 2012. Third pole environment (TPE). Environ. Dev. 3, 52–64.
Zeng, Y.N., Feng, Z.D., 2005. Advances in sandy desertification detecting and its environmental impacts. J. Mt. Sci. 23, 218–227 (in Chinese with English abstract).
Zhang, D.S., Gao, S.Y., Shi, M.Y., Ha, S., Yan, P., Lu, R.J., 2009. Sandy Desertification and Its Control in the Qinghai Plateau. Science Press, Beijing (in Chinese).
Zhang, H.Y., Wang, J.N., Rao, S., 2012. The Study on Ecology Conservation and Environmental Protection in Qinghai-Tibet Plateau. China Environmental Science Press, Beijing (in Chinese).
Zhao, J.X., Qi, B., Duojidunzhu, Shang, Z.H. (2011). Effects of short-term enclose on the community characteristics of three types of degraded alpine grasslands in the north Tibet. Pratac. Sci., 28, 59–62 (in Chinese with English abstract).
Zuo, W.Q., Wang, Y.H., Wang, F.Y., Shi, G.X., 2009. Effects of enclosure on the community characteristics of *Leymus chinensis* in degenerated steppe. Acta Pratac. Sin. 18, 12–19 (in Chinese with English abstract).